ARTICLE

Deconstructing Proton Transport Through Atomically Thin Monolayer CVD Graphene Membranes

Received 00th January 20xx,
Accepted 00th January 20xx

DOI: 10.1039/x0xx00000x

Pavan Chaturvedi,[a] Nicole K. Moehring,[a,b,c] Peifu Cheng,[a] Ivan Vlassiouk,[d] Michael S. H. Boutilier,[e] Piran R. Kidambi[a,b,c,f,*]

Selective proton (H^+) permeation through the atomically thin lattice of graphene and other 2D materials offers new opportunities for energy conversion/storage and novel separations. Practical applications necessitate scalable synthesis via approaches such as chemical vapor deposition (CVD) that inevitably introduce sub-nanometer defects, grain boundaries and wrinkles, and understanding their influence on H^+ transport and selectivity for large-area membranes is imperative but remains elusive. Using electrically-driven transport of H^+ and potassium ion (K^+) we probe the influence of intrinsic sub-nanometer defects in monolayer CVD graphene across length-scales for the first time. At the micron scale, areal H^+ conductance of CVD graphene ~4.5-6 mS/cm^2 is comparable to mechanically exfoliated graphene indicating similarly high crystalline quality within a domain, albeit with K^+ transport ~1 mS/cm^2. However, centimeter-scale Nafion|Graphene|Nafion devices with several graphene domains show areal H^+ conductance ~339 mS/cm^2 and K^+ conductance ~ 23.8 mS/cm^2 (graphene conductance H^+ ~1735 mS/cm^2, K^+ ~47.6 mS/cm^2). Using a mathematical-transport-model and Nafion filled polycarbonate track etched supports, we systematically deconstruct the observed orders of magnitude increase in H^+ conductance for centimeter-scale CVD graphene. The mitigation of defects (> 1.6 nm), wrinkles and tears via interfacial polymerization results in conductance of H^+ ~1848 mS/cm^2, K^+ ~75.3 mS/cm^2 (H^+/K^+ selectivity ~24.5) via intrinsic sub-nanometer proton selective defects in CVD graphene. We demonstrate atomically thin membranes with significantly higher ionic selectivity than state-of-the-art proton exchange membranes while maintaining comparable H^+ conductance. Our work provides a new framework to assess H^+ conductance and selectivity of large-area 2D membranes and highlights the role of intrinsic sub-nanometer proton selective defects for practical applications.

Introduction

Graphene, a monolayer of carbon atoms arranged in a hexagonal lattice, was initially considered to be impermeable to atoms, molecules and ions (at room temperature),[1–6] based on *i)* experiments demonstrating the impermeability to helium (He) gas,[3] and *ii)* theoretical studies predicting high energy barriers (E_B) >3 eV for H,[4,6,7] O,[6] He atoms[2] and $E_B \geq 1.2$eV for proton (H^+) permeation.[4,7] However, Hu et al.[8] measured areal H^+ conductivity ~3 mS/cm^2 (E_B~0.78 eV) as well as no detectable transport of He gas through mechanically exfoliated monolayer graphene suspended over micron-sized apertures and suggested H^+ permeation occurs via holes in the electron distribution in the 2D lattice.[8] While these observations cannot completely exclude the presence of defects smaller than He atoms in the graphene lattice (*i.e.* bond rotation/Stone-Waals defects, point defects etc.) and/or residual polymer/adventitious contaminants adsorbed on defects that could reduce E_B for H^+ transport,[2,9–12] selective proton transport through 2D materials nonetheless, offers fundamentally new opportunities in energy conversion/storage applications as well as novel separations.[1,13–18]

Practical applications will however, necessitate scalable synthesis of monolayer graphene via approaches such as chemical vapor deposition (CVD) that inevitably introduce defects (*e.g.* grain boundaries, intrinsic sub-nanometer(nm) defects, wrinkles etc.) into the 2D lattice and understanding their influence is imperative.[19–27] Defects will likely enhance the transport of protons as well as other species smaller than the defects while limiting transport of larger species via molecular sieving.[12,26,28–32] Indeed, significantly higher proton flux (>10^6 times compared to the pristine lattice) has been calculated[33] to occur via 5757 ring[9,11] defects commonly found along grain boundaries in CVD graphene[11] and high proton fluxes ~1-2 S/cm^2 have been measured through micron-scale disordered graphene (nano graphene and monolayer amorphous graphene) with 7 and 8 membered carbon rings within the lattice with no observable He leakage.[30]

[a] *Chemical and Biomolecular Engineering Department, Vanderbilt University, Nashville, TN, 37212, United States.*
[b] *Interdisciplinary Graduate Program in Materials Science, Vanderbilt University, Nashville, TN, 37235, United States.*
[c] *Vanderbilt Institute of Nanoscale Science and Engineering, Nashville, TN, 37212, United States*
[d] *Center for Nanophase Materials Sciences, Oak Ridge National Laboratory, Oak Ridge, TN, United States.*
[e] *Department of Chemical and Biochemical Engineering, Western University, London, Ontario, Canada, N6A 5B9.*
[f] *Mechanical Engineering Department, Vanderbilt University, Nashville, TN, 37212, United States.*

† Footnotes relating to the title and/or authors should appear here.
Electronic Supplementary Information (ESI) available: [details of any supplementary information available should be included here]. See DOI: 10.1039/x0xx00000x

Further, liquid phase areal proton conductance values for CVD graphene from ~4 mS/cm^2 [29] to ~2.5×10^3 mS/cm^2 (in 0.1M HCl)[28] for micron-scale membranes and from ~1.67×10^3 mS/cm^2 (0.1M HCl)[34] to ~50 ×10^3 mS/cm^2 (1M H_2SO_4)[35] for centimeter-scale membranes along with the transport of larger cations[36–39] such as K^+, Na^+, Li^+ etc. have been observed and attributed to the presence of defects. Such defects in micron-scale monolayer CVD graphene membranes have also been shown to be cation selective.[28,29,38] Ionic selectivity (preferential transport of one species over another) in the case of small defects arises from steric hindrance, surface charge or electrostatic effects from defect edges including termination by O or other atoms, etc., while larger defects can be non-selective (allowing transport of desired and undesired species) and even a small number of such large defects can completely compromise 2D membrane performance.[19]

Although, micron-scale suspended 2D material devices allow for probing defects within an individual graphene domain, and are extremely important for fundamental understanding,[8,28–30,37,38,40–42] practical applications will require large-area graphene membranes where the collective behavior of an ensemble of intrinsic sub-nm defects as well as large defects and any tears from device fabrication will determine the overall performance (proton flux and membrane selectivity). In this context, recent studies have explored the use of Nafion[43] (state-of-the-art proton exchange membrane comprising of a perfluorinated sulfonic acid ionomer) to support 2D materials forming centimeter-scale Nafion|2D material|Nafion or Nafion|2D material devices for applications in isotope separation,[16,17] fuel cells,[13,14] and vanadium redox flow batteries.[15] Here, the use of Nafion as a support enables advancing 2D materials as proton selective membranes for energy applications with improved efficiency by minimizing crossover of undesired species. For example, Bukola et al.[34] reported areal proton conductance ~1.67 S/cm^2 (in 0.1M HCl) and K^+ areal conductance ~10 mS/cm^2 (in 0.1M KCl) using two distinct centimeter-scale Nafion|graphene|Nafion membranes (one for H^+ and the other for K^+). In a subsequent study also using two distinct centimeter-scale Nafion|graphene|Nafion membranes, areal proton conductance ~50 S/cm^2 (in 1M H_2SO_4) and VO^{2+} conductance ~5 mS/cm^2 (in 1M $VOSO_4$) was reported.[17] However, we note the differences in graphene transfer yields/graphene coverage across two distinct membranes (one for H^+ and the other for K^+/VO^{2+}) prevents insights into the origin of enhanced proton transport through centimeter-scale CVD graphene membranes. A recent study by Bentley et al. probing Nafion|graphene membranes via scanning electrochemical cell microscopy (SECCM) in areas that are free from visible large tears and pinholes suggests proton transport occurs primarily via few localized defects in CVD graphene.[44]

We note that the 2-3 orders of magnitude differences between proton conductance values measured over micron-scale and centimeter-scale devices may also result from the differences in quality of CVD graphene used in the different studies and other experimental procedures,[28,29,34,35,39] but the typical cation selective nature of defects in CVD graphene emerges as a common theme.[28,29,38] To the best of our knowledge, no reports exist on proton transport through small and large-scale devices for the same CVD graphene along with insights on the contribution from sub-nanometer scale defects (specifically for large-area membranes), and we aim to bridge this gap in the literature to rationally advance practical applications of 2D membranes.

Here, we systematically probe atomically thin monolayer CVD graphene membranes via ionic conductivity measurements both at small scale (micrometer size suspended membrane) *i.e.* within a graphene domain and large-scale (centimeter-scale Nafion|Graphene|Nafion devices) *i.e.* across multiple domains. Proton conductance of ~4.5-6 mS/cm^2, similar to mechanical exfoliated graphene is obtained for CVD graphene at the micron scale indicating comparable crystalline quality, albeit transport of K^+ ~1 mS/cm^2 is also seen. For centimeter-scale graphene membranes, we observe areal conductance values of ~47.6 mS/cm^2 for K^+ and ~1735 mS/cm^2 for H^+ for CVD graphene in Nafion|Graphene|Nafion sandwich devices which could arise from intrinsic sub-nm defects (< 0.66 nm), small defects (0.66-1.6nm), larger defects (1.6-50 nm) and very large defects such as tears (> 50 nm). We deconvolute the contributions from defects (≥ 1.6 nm), and wrinkles by using Nafion filled well-defined porous polycarbonate track etched membrane (PCTE) supports to isolate large tears (> 50 nm) as well as sealing defects via interfacial polymerization (IP) and attribute the measured areal proton conductance to sub-nanometer-scale proton selective defects (~1848 mS/cm^2 (H^+), ~75 mS/cm^2 (K^+), H^+/K^+ ~24.5). Using a resistance based mathematical model, we explain the presence of large-scale defects along wrinkles and/or tears in combination with sub-nm defects to be responsible for the higher areal proton conductance (~1735 mS/cm^2 for graphene in sandwich membrane and ~ 1848 mS/cm^2 for PCTE membrane) in centimeter-scale membranes in comparison to (~4.5-6 mS/cm^2) micron-scale membranes and demonstrate atomically thin membranes with significantly higher ionic selectivity than state-of-the-art proton exchange membranes while maintaining comparable H^+ conductance.

Experimental

Graphene growth

Graphene was synthesized using atmospheric pressure chemical pressure deposition (APCVD) as published elsewhere.[45–47] Briefly, as received 75 µm-thick copper (Nimrod Copper) was electropolished in a H_3PO_4-based solution and washed with deionized water before drying it with N_2 gas and placed inside a 3 inch diameter quartz tube. To increase the domain size of Cu crystal, electropolished Cu foils was annealed at 1065 °C for 30 min under 500 sccm flow of 2.5% H_2/Ar. Graphene growth was achieved with addition of 0.1% CH_4 (as a carbon source)/Ar and ramping the flow to 20 sccm during 2 h growth duration.

Graphene transfer for micron-scale devices

Single aperture ~2 µm chips in a free-standing silicon nitride membrane window size ~40×40 µm^2 and thickness ~200 nm on ~300

µm thick silicon wafer were purchase from Silson Ltd., UK. A 2 wt% poly (methyl methacrylate) (PMMA, procured from Acros Organics, M.W. 35,000) in Anisole (99% procured from BeanTown Chemical) was spin coated at 1000 rpm for 60s on CVD graphene on Cu foil and the stack was left overnight for drying. Next, the PMMA/Gr/Cu was soft baked at 60 °C for 10-15 minutes. Etching of graphene/Cu was performed in 0.2-0.3M ammonium persulfate (Acros Organics, ACS reagent grade, 98+%). After the complete etching of Cu, the floating PMMA/Gr was transferred to 2-3 water baths to remove the residual ammonium persulfate (APS). Following the water wash, PMMA/Gr was scooped on the silicon nitride membrane. The resulting PMMA/Gr/SiNx was baked at 135 °C for 20 minutes to promote adhesion. Afterwards the PMMA was dissolved using acetone and then washed with isopropyl alcohol(IPA) to minimize the leftover PMMA residue.

Pre-treatment of Nafion membrane and conversion to K^+-form

The as obtained Nafion (here Nafion™ 212, abbreviated as N212 procured from Fuel cell store, Chemours, Nafion™ 212, 50.8 µm thickness) already in proton (H^+) -form was pretreated for 1 h in 0.1 M H_2SO_4 (Fisher ACS Plus 95.5 w/w %), and in de-ionized (DI) water at 80 °C, before soaking the pre-treated Nafion membranes in fresh 0.1 M HCl (Macron Fine Chemicals, 6.0 Normal) for 24 hours to obtain the N212-H^+ form. The K^+-form Nafion was converted from as received H^+-form Nafion by exchanging the protons to potassium ions (K^+). For K^+-form, Nafion membranes were soaked in 0.1 M KCl (99.6%, Fisher Chemical) and KCl solution was exchanged 2-3 times with fresh solution at regular intervals until solution pH was similar to pH of 0.1 M KCl, as reported earlier.[17] Following this, the Nafion membrane was heated at 80 °C in fresh 0.1 M KCl for 1 h before letting it soak in the solution for 48 hours for a complete conversion to K^+-form.[17] The complete conversion to K^+-form is necessary to minimize any possible contribution from protons.

Preparation of Nafion and graphene sandwich membranes

The sandwich N212 samples *i.e.* N212||N212 or N212|Graphene|N212 were prepared as described in previous reports with slight modification.[17] In brief, first graphene (Gr)/Cu was hot pressed (using DABPRESS® 10 ton hand pump at ~825 psi) on the desired form of N212 and after etching of Cu, the second layer of N212 was hot-pressed on N212|Gr, completing the Nafion graphene sandwich membrane denoted as N212|Gr|N212. PTFE-coated fiber glass fabric sheets (McMaster-Carr thickness ~ 0.010") were used as a support for Gr/Cu during transfer onto Nafion to avoid the direct contact with the metal surface of hot-press machine and a Silicon rubber gasket was used for even pressing of the Gr/Cu on Nafion.

Ionic conductance measurements

Ionic conductance values were extracted from the current-voltage (I-V) curves which were obtained from the multi-chronoamperometry measurements either in a two-electrode (for small scale) or 4-electrode (for large scale) configuration, as shown in Fig. 1 and Fig. 2. In a 4-electrode geometry, Pt wires (procured from Alfa Aesar, 0.25mm diameter, 99.9%) work as counter and working electrode whereas Ag/AgCl pellet electrodes (purchased from A-M Systems) work as reference and working-sense electrodes. Two-electrode measurements were performed using homemade Ag/AgCl electrodes. Here, prior to recording current/voltage in steps of 10-20 mV (multi-step chronoamperometry) each for 30-60 s, a stable open circuit potential was acquired (usually 120-300 s). For the small-scale (suspended graphene membranes on micron scale apertures) measurements, wetting of the graphene membrane was achieved by filling both the reservoirs first with ethanol, followed by 50% ethanol and then slowly exchanging with pure water before filling it with the desired electrolyte solution.[37] All the solutions were double filtered and degassed prior to their use and the measurements were performed inside a Faraday cage. Large scale conductivity measurements were also performed in a custom-made H-cell with internal diameter of 9 mm. Here, precaution was taken to ensure there were no air bubbles inside the capillary.

Areal conductance, $S= G /A$, was obtained from the *I-V* curves where conductance, $G=I/V$ (slope of the linear portion of the *I-V* curves) $=1/R$, R being the resistance of the membrane and A is the active area of the membrane ~ 0.68 cm^2. The resistance of individual elements such as Nafion sandwich and graphene were estimated based on a series resistance model. For example, resistance (estimated from *I-V*) for sandwich membrane N212|Gr|N212, $R_{N212|Gr|N212+Solution}$ will have the contribution from solution resistance and thus the total resistance can be written as a sum of solution resistance ($2\times R_S$), nafion sandwich (N212||N212; two layers of N212) resistance ($2\times R_{N212}$) and graphene resistance (R_{Gr}) (also shown in Fig. 2B) *i.e.*

$$R_{N212|Gr|N212+Solution} = 2 \times R_S + 2 \times R_{N212} + R_{Gr} \quad (1)$$

The individual element "graphene (Gr)" resistance can be estimated by rearranging equation (1) as,

$$R_{Gr} = R_{N212|Gr|N212+Solution} - (2 \times R_S + 2 \times R_{N212}) \quad (2)$$

Thus, obtained graphene resistance (R_{Gr}) can be used to calculate areal conductance of graphene, S_{Gr} as

$$S_{Gr} = \frac{G_{Gr}}{A} = \left(\frac{1}{R_{Gr}}\right) \times \frac{1}{A} \quad (3)$$

Table S1 summarizes details of samples and their nomenclature.

Chemical and Electro-chemical etch tests for defect analysis

For the defect analysis of the graphene, etch test was performed using 0.1 M $FeCl_3$ (purchased from EMD Millipore Corporation, Assay > 98.0%) solution in DI water for a time of 5 s before washing the Gr/Cu with plenty of DI water to completely wash off the residual $FeCl_3$ as reported elsewhere.[19] Electrochemical etch test was performed in a two-electrode geometry using 0.5 M $CuSO_4$ solution at an applied potential of 1 V for 1 s where graphene/Cu works as a working electrode and another copper piece as a counter and reference electrode.

Raman spectroscopy

Raman measurements were performed using a confocal Raman microscope (Thermo Scientific DXR) with a 532 nm wavelength laser and a 900 lines/mm grating. The collection parameters were an exposure of 5 s and averaging of 30 scans with a spot size of 1.1 µm (50X microscope). The laser power was kept at 8 mW. The spectrum resolution was 5.5-8.3 cm^{-1} for the current experimental conditions.

Graphene transfer on polycarbonate track etched (PCTE) membranes

Graphene was transferred onto PCTE membranes using IPA assisted hot lamination procedure following the previously reported protocols.[24] First, APCVD graphene on Cu foil was pre-etched in 0.2 M APS solution for 2.5 hours to remove the graphene on the backside as well as reduce the thickness of the Cu foil, followed by floating on DI water (2 times for 10 min each step) and drying in air. Polycarbonate track etch (PCTE, Sterlitech, ~9.4-10% porosity, 10 µm thick, hydrophobic, polyvinylpyrrolidone-free) substrate was also washed in pure ethanol (Sigma Aldrich, 200 proof) and dried in air. A thin layer of isopropanol (IPA) solvent was introduced to PCTE and graphene/Cu interface as the heat transfer medium. Following this, the stack of paper/PCTE/Gr/Cu/paper was sandwiched between two protective Teflon films and then laminated at 135 °C using a TruLam TL-320B roll-to-roll compatible laminator. Subsequently, the PCTE/Gr/Cu was gently made to float on APS solution to completely etch Cu. Finally, the PCTE/Gr stack was rinsed with DI water to remove the APS residue, followed by rinsing in ethanol and drying in air.

Interfacial polymerization (IP) process

Interfacial polymerization was carried out based on the previous reports.[24,25] In brief, PCTE/Gr was assembled in a Franz cell (PermeGear, Inc.; Inner diameter 15 mm) and IP process was performed using octa ammonium polyhedral oligomeric silsesquioxane (POSS, Hybrid Plastics, AM0285) in water (aqueous phase) and trimesoyl chloride (TMC, Alfa Aesar, 4422-95-1) in hexane (organic phase) for 1 hour.

Filling Nafion within PCTE supports

The PCTE pores were filled with Nafion by dipping into a solution of 2.5 wt% Nafion (total volume 1.5 mL; diluted from 5 wt% (D520, Fuel Cell Store) in IPA) for 25 minutes and subsequent drying under ambient conditions. This Nafion dip coating step was repeated once more with 5wt% Nafion solution. After Nafion dip coating the thickness of PCTE membranes were 14±2 µm. The thickness was measured across the membrane at multiple points (4-5 points per sample) using a digital micrometer with an accuracy of ±1 µm. The K^+-form conversion was achieved by soaking the nafion filled PCTE membranes in multiple 0.1M KCl solutions over 48 hours.

Results and discussion

Micron-scale suspended graphene membranes

Initially, we probe proton (H^+) and potassium ion (K^+) transport through micron-scale suspended CVD graphene membranes. Here, CVD graphene was suspended on ~2 µm diameter aperture in silicon nitride/Si wafer (see experimental section) and assembled into a custom-built cell equipped with inlet/outlet ports for the electrolyte and Ag/AgCl electrodes (see Fig. 1A inset for cell schematic). SEM image of the CVD graphene membrane (see inset in Fig. 1A) shows uniform contrast with some minor polymer residue (indicated via arrows) from transfer visible towards the edges of the membrane. We note that complete removal/elimination of residual polymer is non-trivial[48–54] and refrain from heating the transferred CVD graphene in H_2 or employing aggressive cleaning procedures to avoid inadvertent introduction of defects into the graphene lattice that could influence transport measurements. Fig. 1A shows a representative multi-step chronoamperometry plots for a graphene membrane for different electrolytes and Fig. 1B shows current-voltage (I-V) curves extracted from Fig. 1A after open circuit potential (potential corresponding to zero current) correction. The linear portion of the I-V curve is used to calculate the conductance, $G = I/V$ and corresponding area normalized conductivity $S=G/A$, where A is the area of the suspended membrane (Fig. 1C). The measured areal conductance values of ~4.5-6 mS/cm^2 for 0.1 M HCl are in agreement with the previously reported values for exfoliated[8,40,42] and CVD graphene[29] (Fig. 1C), indicating comparable crystalline quality[55] of our CVD graphene over micron-scale areas (within a single graphene domain, typically ~100µm our CVD graphene[46,47]). Interestingly, despite comparable H^+ conductance to exfoliated graphene, we also observe transport of K^+ (hydrated ion diameter ~0.66nm) ~1 mS/cm^2 for the same graphene membrane at micron-scales.[29,38]

The measured conductance is significantly lower (at least 50×) than the diffusion limited current for a 2 µm open aperture (see supporting information for details). Further, a lower limit of current of ~1-3 pA at 1 V (Fig. S1) was measured for a closed chip, indicating that our measurements are well above the limit/threshold of the experimental set-up. Higher conductance values occasionally observed for some samples (not shown here) for both protons (H^+) and potassium ions (K^+) suggest the presence of large defects.

An estimation[56] of conductance using

$$G = \sigma \times \left(\frac{4t}{\pi * d^2} + \frac{1}{d}\right)^{-1} \quad (4)$$

where $\boldsymbol{t}$ is the commonly used thickness of graphene in an electrolyte solution ~0.68 nm,[57] d is the defect diameter, and σ is the conductivity of the solution, results in an equivalent single defect ~0.3 nm in size (representing the measured conductance) for samples shown in Fig. 1C. Here, we acknowledge that the simplistic assumptions such as conductivity σ inside a nanopore/defects is the same as bulk conductivity and the presence of no surface charges on the pore/membrane can potentially lead to some deviations in the estimated defect size. Further, the nanopore/defect conductivity can also change appreciably when the defect size is comparable to the ionic size of the permeating species due to a decrease in the

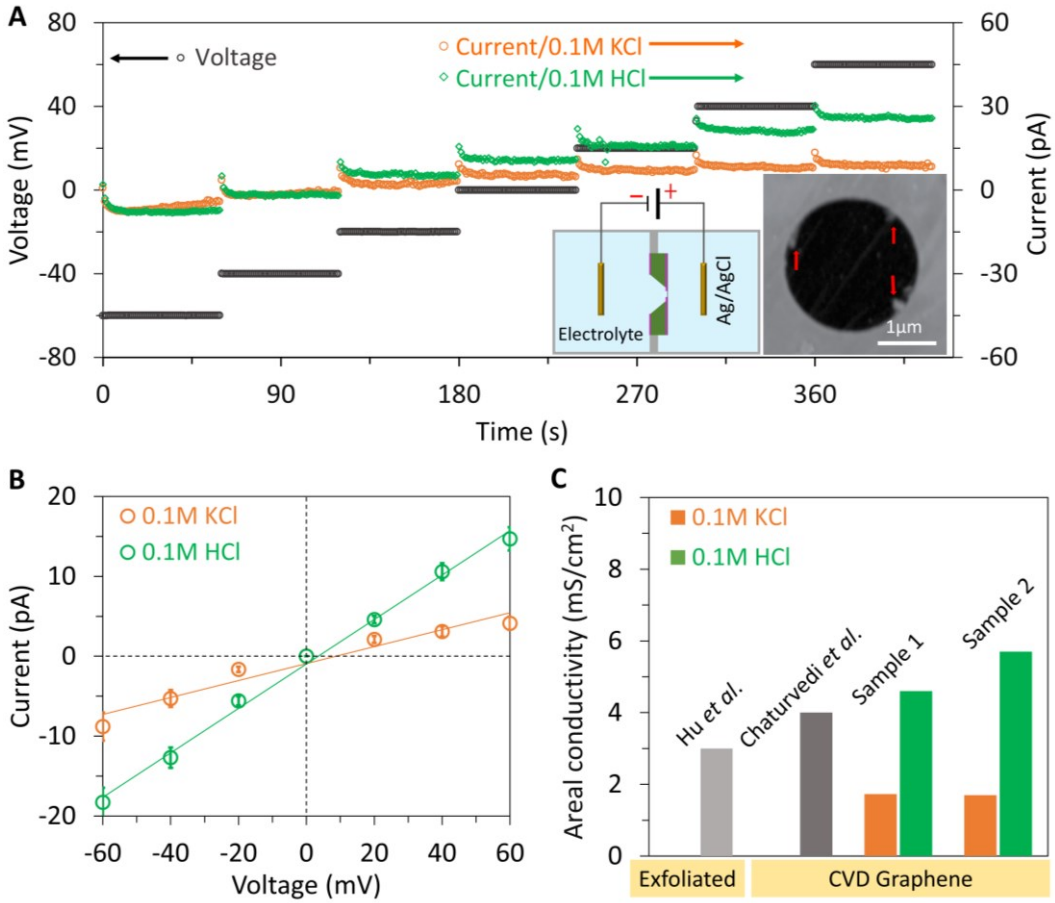

Fig. 1 Ionic transport through micron-scale monolayer graphene membranes. A) Representative multi-chronoamperometry current-voltage plots current in 0.1 M HCl (green) and 0.1 M KCl (orange) and voltage (black). Insets show the schematic of the 2-point measurement set-up and SEM image of suspended monolayer graphene covering an aperture in 200 nm SiN_x coated Si wafer. Red arrows point the polymer residues. B) Representative I-V curves (extracted from multi-chronoamperometry in A after correction for open circuit potential) for 0.1 M HCl (green) and 0.1 M KCl (orange) on the same graphene membrane for sample 1. C) Areal conductance for CVD graphene samples computed from B along with literature values for exfoliated graphene (Hu et al.~3 mS/cm^2) measured using 0.1 M HCl and CVD graphene (Chaturvedi et al.~4 mS/cm^2) measured using 0.1 M HCl + 0.1 M KCl.

concentration of ions inside the nanopore/defect and lower ionic mobility.[56] Higher H^+ conductance values could also arise due to the presence of large defects (that can allow K^+ transport) as well as multiple small defects (that may not allow K^+ transport).

The observed transport of K^+ ions for the CVD graphene (Fig. 1C) even while the proton conductance values remain comparable to mechanical exfoliated graphene can be explained by *i)* residual protons in 0.1 M KCl (the pH of 0.1 M KCl solution was ~5.3, but measurements using 0.001 M HCl showed lower conductance of ~ 1.3 mS/cm^2), so we exclude it as a possible explanation, *ii)* via the presence of defects or charges on the defect edges as well as *iii)* any potential changes to the hydration shell around the K^+ ions that allow it to transport through defects <0.66 nm. Here, we note that Qi et al[40] measured areal proton conductance ~12 mS/cm^2 and ~10 mS/cm^2 of NaCl conductance through the same mechanically exfoliated graphene membrane and ascribed it to defects as well as potential system leakages in comparison to ~3 mS/cm^2 proton conductivity reported by Hu et al[8] for mechanically exfoliated graphene (where transport of other cations was not studied). Based on the measured proton conductance values, we conclude that the quality of our CVD graphene over micro-scale areas (graphene domain size ~100 µm[46,47] and potential absence of grain boundaries and associated defects etc.) is comparable to that of mechanically exfoliated graphene for proton transport.

Centimeter-scale Nafion|Graphene|Nafion sandwich membranes

Next, we proceed to probe proton transport over large areas (centimeter-scale) through the same CVD graphene by sandwiching it between Nafion. Prior to CVD graphene transfer on Nafion (N212^{TM}, ~50 µm thick), the as received Nafion (labelled as N212) was converted to either protonated (H^+) form (labeled as N212-H^+) or potassium ion (K^+) form (labeled as N212-K^+) (see methods).[17] CVD graphene (Gr) on copper foil was transferred to N212 via hot-pressing, as shown in the Fig. 2A, (also see experimental section) followed by etching of the Cu foil and finally another layer of Nafion

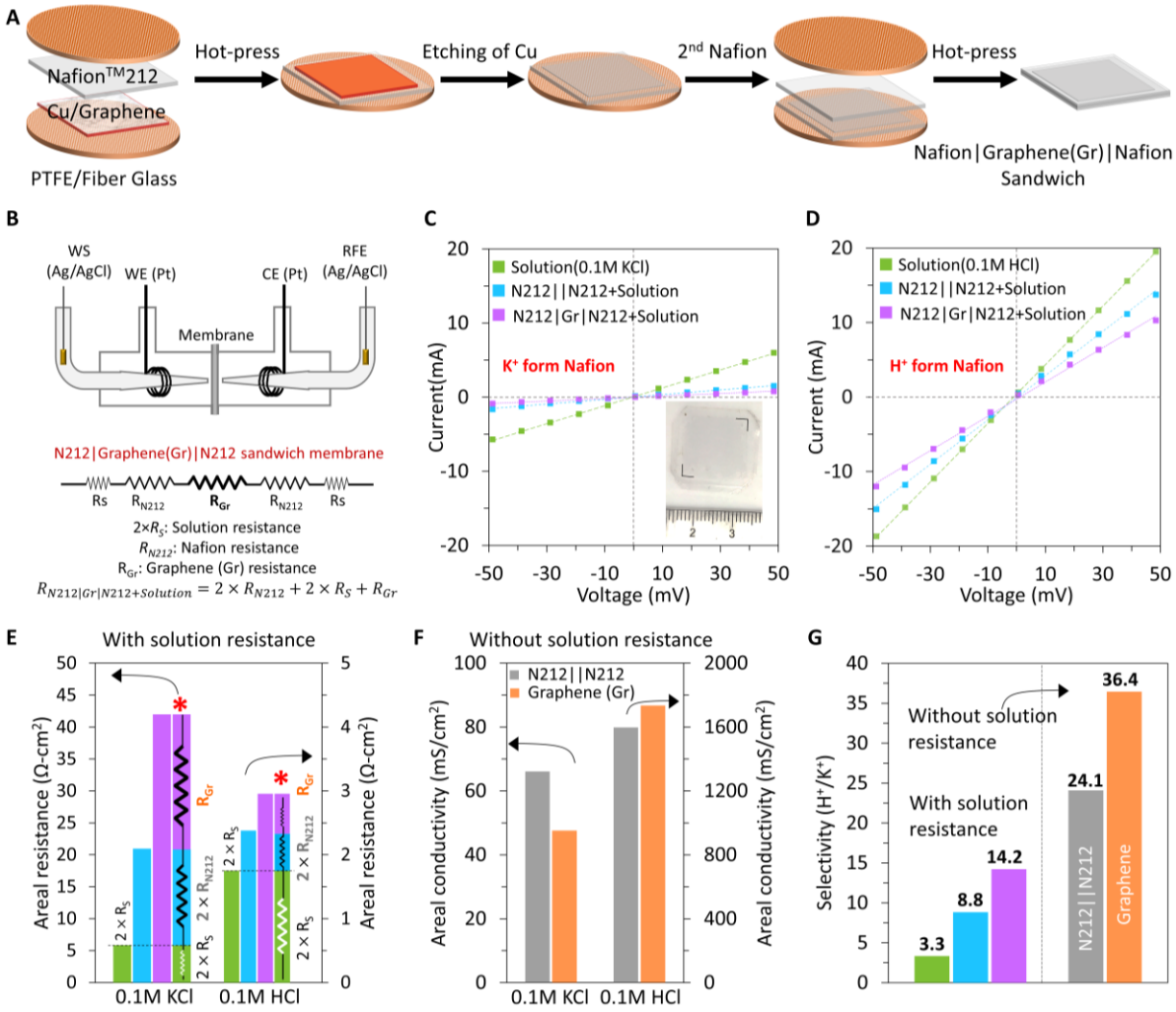

Fig. 2 Ionic transport through centimeter-scale monolayer graphene membranes. A) Schematic of CVD graphene transfer to Nafion (N212) support and fabrication of centimeter-scale graphene (Gr), Nafion (N212) sandwich membranes (N212|Gr|N212). B) Schematic of 4-electrode measurement set-up and equivalent resistance model of the N212|Gr|N212 membrane. Current-voltage (*I-V*) curves for sandwich membranes with graphene N212|Gr|N212 (purple) and N212||N212 (blue) after converting N212 to the C) K^+ form and D) H^+ form. Inset in C) shows optical image of the N212|Gr|N212 sandwich membrane with the dark square indicating graphene. E) Areal resistance of solution (green), "N212||N212+solution" (blue) and with graphene "N212|Gr|N212+solution" (purple). The bar with the * is a guide for the eye and indicates resistance contributions from individual components in the N212|Gr|N212 sandwich membrane measurements *i.e.* solution resistance (green, $2 \times R_S$), resistance from Nafion N212||N212 (blue, $2 \times R_{N212}$) and resistance from graphene (purple, R_{Gr}). F) Areal conductance values computed by taking the inverse of resistance values of graphene only (R_G, orange, graphene resistance after solution resistance subtraction) and Nafion sandwich only ($2 \times R_{N212}$, grey, after solution resistance subtraction) in E. G) Selectivity (H^+/K^+) computed by taking the inverse of the ratio of areal resistance for solution (green), "N212||N212+solution" (blue) and "N212|Gr|N212+solution" (purple) in E) as well as the ratio of areal conductance values for graphene (Gr, orange) and Nafion sandwich (N212||N212, grey) without solution contribution in F) for H^+ and K^+, respectively. Also see supporting information Table S2 for measured values. All the H^+ and K^+ measurements are performed in 0.1M HCl and 0.1M KCl respectively.

was hot pressed on the graphene to result in the centimeter-scale Nafion|Graphene|Nafion membranes (labelled as N212|Gr|N212). The N212|Gr|N212 membrane was assembled into a custom-built H-cell (Fig. 2B, S2A) for ionic conductivity measurements performed in a 4-electrode configuration (see experimental section) to aid accurate measurements of solution and membrane resistance. Fig. 2C,D, show I-V curves for open cell, N212||N212 and N212|Gr|N212 membranes in 0.1M solution/electrolyte in K^+ and H^+ forms respectively via exchanges describe earlier. The control membranes exhibit distinctly different areal ionic conductance of ~47 mS/cm² (K^+) and ~420 mS/cm² (H^+) due to the difference in transport rates for H^+ and K^+. The addition of graphene in between the N212 i.e. N212|Gr|N212 sandwich membrane, hinders the transport of both K^+ and H^+ ions as observed by increase in the effective resistance or

decrease in the measured ionic current (Fig. 2C, D). The normalized areal resistance (R_A) for the membranes (Fig. 2E) is obtained from the I-V curves by first taking the slope of the linear region to obtain conductance (σ), σ=I/V and then taking the inverse of conductance σ=1/R to obtain resistance (R) and finally multiplying the resistance by the active area (A) of the membrane ~0.68 cm^2 i.e. R_A= R×A. Fig. 2E shows the area normalized resistance for solution (K^+ ~5.8 Ω-cm^2, H^+ ~1.8 Ω-cm^2), Nafion control (K^+ ~21.0 Ω-cm^2, H^+ ~2.4 Ω-cm^2), and N212|Gr|N212 sandwich membranes (K^+ ~42.0 Ω-cm^2, H^+ ~3.0 Ω-cm^2), for both K^+ (in 0.1 M KCl) and H^+ (in 0.1 M HCl) ions as well as individual contribution from each elements in the equivalent electrical circuit towards the total N212|Gr|N212 membrane resistance indicated by * in Fig. 2E.

The normalized areal conductance for N212||N212 sandwich (after subtracting contribution from solution resistance) and graphene (Gr) (after subtracting contribution from Nafion sandwich and solution resistance) are obtained from the inverse of the individual element areal resistance values (using electrical model presented in Fig. 2B) and are presented in Fig. 2F (also see Table S2). The N212||N212 and graphene (Gr) membranes show areal conductance of ~66 mS/cm^2 and 47.6 mS/cm^2 respectively at 0.1 M KCl while the areal proton conductance values measured at 0.1 M HCl are ~1600 mS/cm^2 and ~1735 mS/cm^2, respectively. Selectivity, defined as the ratio of H^+ to K^+ conductance is also presented in Fig. 2G and the addition of graphene increases the selectivity from 8.8 (Control) to 14.2 (Graphene sandwich membrane), signifying an improvement in proton selectivity after the addition of graphene arising from enhanced hindrance to K^+ ions. Finally, we compute a selectivity ~36.4 for monolayer CVD graphene (Gr) in comparison to ~24.1 for N212||N212 membranes (Fig. 2G) after subtracting the contribution from electrolyte (see Table S2).

Notably, the areal conductance changes substantially from micron-scale to centimeter-scale CVD graphene membranes for both H^+ (~4.5-6 to ~1735 mS/cm^2) and K^+ (~2 to ~45 mS/cm^2). We specifically performed the K^+ and H^+ measurements on the same membranes via facile exchange of cation in this study to conclusively exclude any variations from the graphene transfer yield or sample to sample variations from processing steps. We further note the lower limit on the probed defect size is ~0.66 nm (the hydrated diameter of K^+ ions). Proton conductance of ~1735 mS/cm^2, similar to ~1667 mS/cm^2 as reported by Bukola et al[17] for centimeter scale CVD graphene (albeit significantly higher than the micron-scale graphene membranes with proton conductance of ~4.5-6 mS/cm^2) but distinctly different K^+ conductance suggest possible differences in graphene quality with a complex nature of sub-nm defects, larger defects and coverage of graphene as well as other factors such as doping and strain on the graphene.

Defect analysis of CVD graphene

Compared to micron-scale membranes, large scale transfers of graphene will have additional defects such as wrinkles and associated ~50 nm defects, domain boundaries patched by different carbon-membered rings (575, 585 carbon rings), sub-nm defects such as single, multi-carbon vacancies as well as tears from the sample preparation/transfer processes.[9,19,24,25,58] These defects will contribute towards the measured ionic transport as well as the resulting selectivity. A facile approach for analyzing defects in CVD graphene on Cu over large areas utilizes etchants such as iron chloride ($FeCl_3$) or ammonium persulfate (APS) to etch copper underneath the defects.[19] Acid etch test using 0.1 M $FeCl_3$ for 5s reveals the defects in CVD graphene as etch pits (Figs. 3A,B).[59] Assuming each etch pit corresponds to a single defect, an analysis (Fig. S3) of the SEM image via ImageJ provides a bimodal distribution of etch pits with an estimated defect density ~7.1×10^6 defects/cm^2 (Fig. 3C). An increased defect density of ~8.6×10^6 defects/cm^2 is estimated for electrochemical etch test (which can probe defects smaller than the acid etch test) which is slightly higher than the defect density of ~7.1×10^6 defects/cm^2 for the acid etch test.[19] We note that the etch pits appear to line up along wrinkle like features in the CVD graphene consistent with the propensity of defect clustering along wrinkles reported in prior studies.[19,24]

SEM images of the large area CVD graphene transferred onto N212 (Fig. 3D) do not show visible cracks or tears and shows uniform contrast without polymer charging indicating successful high yield transfer. The presence of dark contrast features consistent with wrinkles cover ~1.66% of the total area and is in broad agreement with wrinkle areal fraction of ~0.2-0.6% in the as-synthesized CVD graphene on Cu (assuming an upper bound on the width of wrinkles as ~50 nm). We note that prior studies suggested larger defects ~4-50 nm show a preference to cluster along wrinkles which is also observed from the propensity of etch pits to cluster along wrinkles (Fig. 3B).[24] Wrinkles are also prone to tear/damage during the sandwich membrane preparation which will result in tears >50 nm. Further, the preparation of sandwich membranes via hot-press and subsequent hydration of the Nafion may introduce mechanical strain in the transferred CVD graphene due to the difference in thermal expansion coefficients of Nafion (~9×10^{-4}/°K)[60] and graphene (-8×10^{-6}/°K)[61] which could result in cracks/tears. However, we do not observe any significant cracks or tears in the CVD graphene transferred to Nafion from the SEM images (Fig. 3D) and hence consider any influence from such secondary effects to be minimal.

Raman spectra of graphene transferred to Nafion, N212 (in K^+ form) and to SiO_2/Si wafer shows the characteristic peaks (Fig. 3E) ~1350 cm^{-1} (D), ~1590 cm^{-1} (G) and ~2680 cm^{-1} (2D). The ratio of intensity of D to G peak, I_D/I_G ~0.02 indicates high quality graphene[62] with negligible defects and the I_{2D}/I_G >1 with a 2D peak full-width half maxima (FWHM) of ~30 cm^{-1} confirms transfer of monolayer graphene on SiO_2.[19,22,67–71,24–26,54,63–66] Unfortunately, the overlap of the characteristic peaks of Nafion with the position of the D-peak hinders information on defects in CVD graphene after transfer to Nafion via Raman spectroscopy (as shown in Fig. 3E). Raman spectra of graphene on N212 (Fig. 3E), however, indicates p-doping of graphene via a shift of the G peak towards higher wavenumbers by ~20 cm^{-1}, 2D peak shift by ~ 10 cm^{-1}, a change of ~10 cm^{-1} in the FWHM of G-peak, and a decrease in the intensity ratio of 2D to G, I_{2D}/I_G from 2.67 to ~1.4 in comparison to graphene transferred on

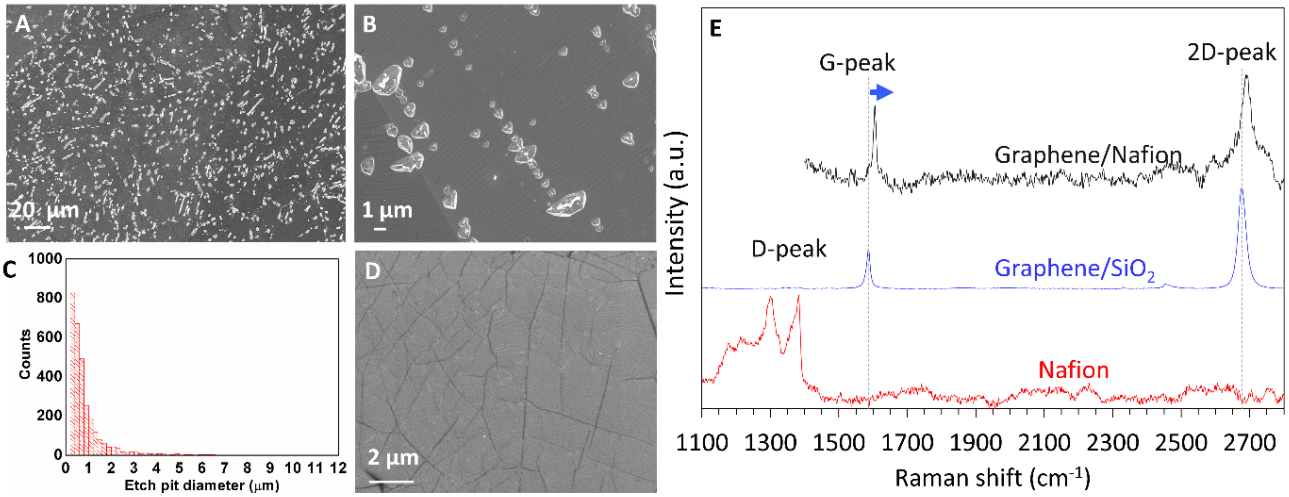

Fig. 3 Defects in large-area monolayer CVD graphene. A, B) SEM images of graphene on Cu foil after an acid-etch test with 0.1 M $FeCl_3$ for 5 s. The electrochemical test in B) shows smaller size etch pits and the etch pits appear to align with features consistent with wrinkles in the CVD graphene. C) Diameter distribution of etch pits extracted from A) using ImageJ software. D) SEM image of large-area graphene transferred on to the Nafion (N212) identified via the presence of wrinkles in the graphene. E) Raman spectra for the graphene transferred on 300 nm SiO_2/Si wafer (blue) and Nafion 212 (black). The black vertical lines correspond to the characteristic 2D (~2700 cm^{-1}), G (~1600 cm^{-1}) and D (~1350 cm^{-1}) peaks in graphene. The overlap of Nafion peaks over the D peak region prevents collection of Raman spectra in those regions for graphene transferred on to Nafion.

the SiO_2/Si substrate.[72] The p-type doping is attributed to charge transfer based doping from the sulfonic groups (SO_3^-) in Nafion.[73,74]

Polycarbonate track etched (PCTE) Support for Mitigating Large Tears/Defects

The presence of even a small fraction of tears in centimeter-scale graphene membranes could allow for significant K^+ flux and wrinkles typically have clusters of large non-selective defects present which could allow for K^+ flux as well. The presence of defects and tears in CVD graphene transferred to Nafion is also reported by Bentley et al., where they show enhanced proton conductance.[44] Here, we deconstruct the influence of wrinkles and tears by leveraging the well-defined porous polymer support such as polycarbonate track etched (PCTE with ~200 nm cylindrical straight channel pores) membranes to support graphene and use interfacial polymerization (IP) to seal the large tears/defects (Fig. 4A).[24–26] Our own prior studies have shown negligible K^+ transport through PCTE+Gr+IP membranes.[24,25]We calculate a defect size of ~1.6nm in the CVD graphene supported on a ~200nm diameter PCTE support pore will exhibit transport characteristics similar to a completely open/uncovered ~200 nm pore (*i.e.* a single ~1.6nm defects will manifest as a tear of size ~200 nm diameter PCTE support pore) and exhibit selectivity as well as ionic conductivity similar to bulk electrolyte (see supporting information for details).

Fig. 4A shows a schematic of the isolation of tears and wrinkles via CVD graphene transfer to PCTE support with ~10% porosity and subsequent sealing (via interfacial polymerization(IP)) as well as finally dip coating the CVD graphene (Gr)+PCTE+IP membrane with Nafion (to facilitate an effective comparison with the Nafion|Gr|Nafion sandwich membranes). The variation from graphene coverage (despite typically high transfer yields >96%) limits effective controls since the amount of IP and the transport characteristics of the IP plugs may be different each membrane, thereby preventing precise delimiting of the ionic resistance/conductance of individual elements (PCTE, CVD graphene and Nafion) similar to Fig. 2E and F. Therefore, no correction of solution resistance or Nafion was performed for the PCTE measurements to estimate the resistance/conductance of CVD graphene "only". The areal resistance (Fig. 4B, Table S3) for Nafion filled PCTE (~0.24 Ω-cm^2 for H^+ and ~2.1 Ω-cm^2 for K^+) and Nafion filled PCTE+graphene (~0.27 Ω-cm^2 for H^+ and ~2.8 Ω-cm^2 for K^+) membranes show a minor increase in the resistance for H^+ (~13%) and K^+ (~33%) ion transport with the addition of graphene on PCTE membrane, suggesting contribution from defects >1.6nm that overlap the PCTE support pores.[24–26,58] To rule out the possibility of a small number of such larger defects and tears overwhelming ionic transport in comparison the sub-nm defects, we use interfacial polymerization (IP) to selectively form polymer plugs and seal the large defects/tears and defects overlapping the PCTE pores (see methods).[25] After sealing the defects (>1.6 nm) via IP (Fig. 4B), the areal resistance for PCTE+Gr+IP+Nafion increases to ~0.54 Ω-cm^2 for H^+ and ~13.3 Ω-cm^2 for K^+ in comparison to PCTE+Gr ~0.27 Ω-cm^2 for H^+ and ~2.8 Ω-cm^2 for K^+, which corresponds to a resistance increase of ~100% (H^+) and ~475% (K^+) after IP. Such a significant increase in the areal resistance for both H^+ and K^+ suggests effective sealing of

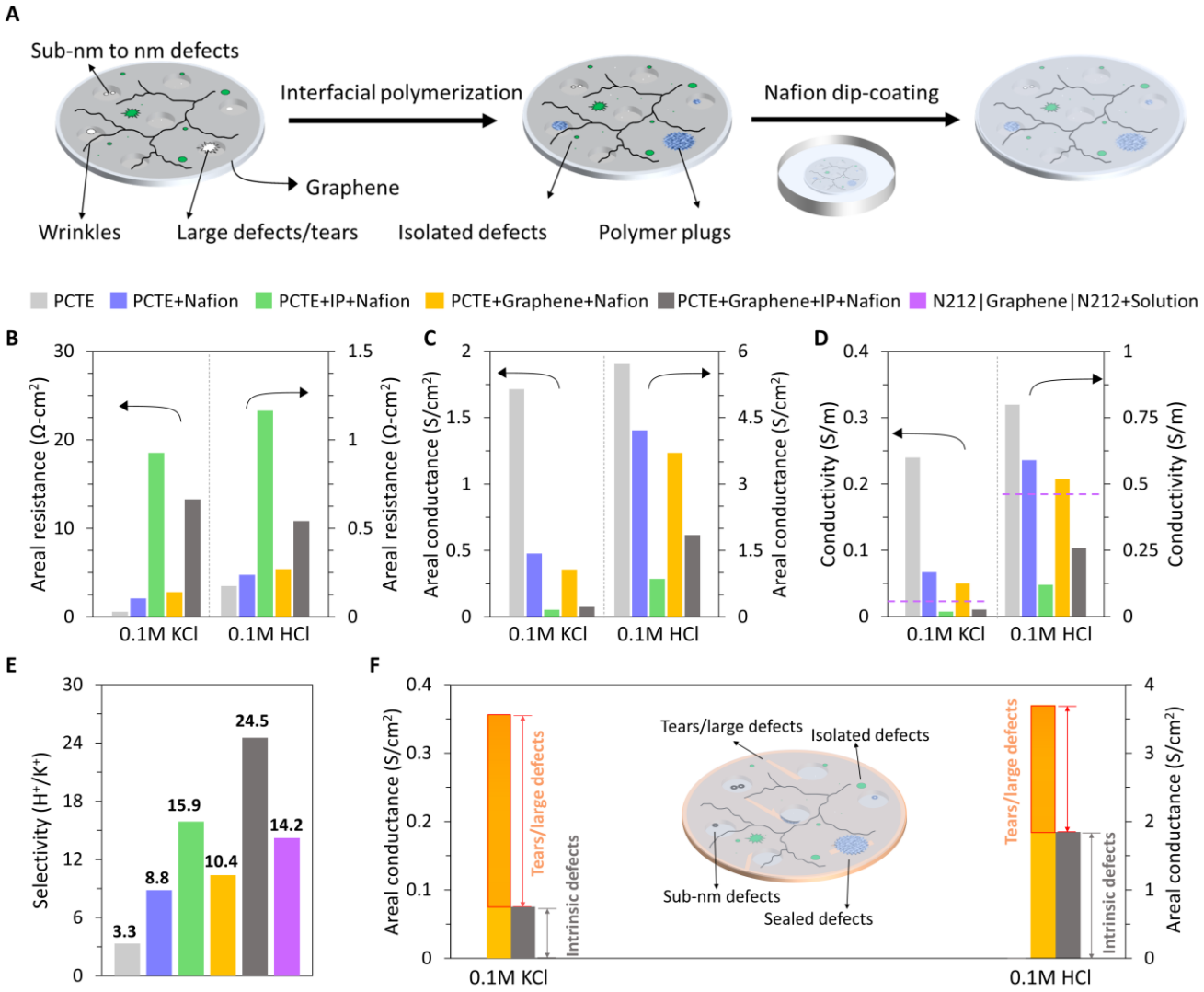

Fig. 4 Understanding the contribution of defects in ionic transport through centimeter-scale monolayer graphene membranes. A) Schematic showing centimeter-scale graphene transferred to polycarbonate track etched (PCTE) supports (~9.4-10% porosity ~200 nm pores) to isolate wrinkles and large tears and minimize contributions to ionic transport from them. Subsequent interfacial polymerization (IP) allows for sealing of large defects (>0.5-0.66 nm) and tears in graphene. Finally, the PCTE + Gr + IP membrane is dip coated in Nafion to facilitate a direct comparison with graphene sandwiched between Nafion 212 supports (see Fig. 2). B) Areal resistance (Ω-cm^2), C) Areal conductance (S/cm^2), D) Conductivity (S/m), E) H^+ / K^+ selectivity for PCTE supports (grey), PCTE with Nafion filled into the channels via dip coating (PCTE + Nafion), PCTE with graphene and subsequent Nafion filling of the PCTE channels (PCTE + Gr + Nafion), and PCTE with graphene subjected to interfacial polymerization (IP) and filled with Nafion (PCTE + Gr + IP + Nafion). Note unlike Fig. 2F the areal conductance values in Fig. 4B include contribution from solution *i.e.* 0.1 M HCl and 0.1 M KCl for measurements of H^+ and K^+ transport, respectively., since the IP plugs formed with graphene could exhibit different transport characteristics than IP plugs formed within bare PCTE. The dip-coated Nafion is converted to K^+ form or H^+ form prior to the corresponding measurements (see methods). The dotted purple lines in D) shows values on Nafion 212 sandwich with graphene (N212|Gr|N212 + solution) extracted from Fig. 2E for an effective comparison between graphene transferred to PCTE or Nafion 212 supports, respectively. F) Deconstruction of contribution from intrinsic defects and large defects towards the overall conductivity for PCTE+Gr+Nafion (yellow) and PCTE+Gr+IP+Nafion (grey) using areal conductance values from Fig. 4C and schematic of defects within graphene transferred onto the PCTE support. Also see supporting information Table S3 for measured data values.

larger defects as well as tears, mitigating their contribution towards the measured ionic transport.

Fig. 4C shows the areal conductance values for different membranes obtained by taking the inverse of the areal resistance from Fig. 4B. Although the areal conductance of PCTE+Gr+Nafion (~3703 mS/cm^2 for H^+ and ~356 mS/cm^2 for K^+) is significantly higher than the N212|Gr|N212 sandwich membrane (~339 mS/cm^2 for H^+ and ~ 24 mS/cm^2 for K^+), upon considering the differences in membrane

thicknesses (see Fig. S5), the conductivity (S/m) values for both these membranes appear to be in good agreement (Fig. 4D). The areal conductance of PCTE+Gr+IP+Nafion membrane is ~1848 mS/cm^2 for H^+ and ~ 75 mS/cm^2 for K^+ which corresponds to a selectivity of 24.5 (Fig. 4E). Fig. 4F compares the measured H^+ and K^+ areal conductance for PCTE+Gr+Nafion (yellow) and PCTE+Gr+IP+Nafion (grey) membranes to illustrate the efficacy of IP process in isolating the contribution to conductance from larger defects and tears. The significantly higher selectivity of 24.5 for PCTE+Gr+IP+Nafion membrane compared to 14.2 for N212|Gr|N212 sandwich membranes, suggests that large non-selective defects are effectively blocked by the IP and the sub- nm proton selective defects (smaller than the IP plugs) govern the membrane selectivity. We further note that the thickness of PCTE+Gr+IP+Nafion membrane is ~14 µm and yet it shows superior ionic selectivity ~24.5 compared to ~100µm thick N212||N212 with ionic selectivity ~8.8, while still maintaining comparable proton conductance.

Mathematical Transport model

Since the measured H^+ conductance through centimeter-scale Nafion|Gr|Nafion as well as PCTE+Gr+IP+Nafion (~1.74 – 1.84 S/cm^2) is significantly higher than the H^+ conductance of the graphene measured at the micron-scale (~4.5-6 mS/cm^2), transport of H^+ occurs through more pathways than just through the lattice to account for the measured graphene selectivity on the larger scale. To consider the influences of defects and tears in the large-area graphene we develop a mathematical model. While intrinsic defects are typically nanometer scale and form during graphene synthesis, larger defects up to ~50 nm commonly form along wrinkles in graphene.[24,58] We consider the possibility of conductance through both tears and defects by adding their contributions in parallel (Fig. 5A) and model them using the simple graphene conductance model (Eq. 1). In this model, there are two contributions to the resistance limiting ion flux through each graphene pore (Fig. 5B).[56] The first is the resistance to passing through the pore due to its low area compared to the bulk, R_{pore}. The second term is the resistance ions experience accessing the pore, R_{access}. This occurs because the graphene in between pores has low ion conductance, forcing ions to funnel toward the pores to pass through the membrane. However, when applying this conductance model to the N212|Gr|N212 membrane, it is important to note that because the graphene has Nafion directly on either side, the access resistance experienced by ions passing through the graphene occurs in the Nafion rather than in the bulk solution. The mobility, and hence the effective conductivity, of H^+ and K^+ are both lower in Nafion. The ion conductivities in the Nafion are calculated by multiplying the Nafion||Nafion areal conductivity by the membrane thickness, resulting in $\sigma_{H^+} = 1.6$ S/m and $\sigma_{K^+} = 0.067$ S/m. These conductivity values are used in the model calculations below.

The total conductance (G) is calculated as,

$$\frac{G}{A} = \frac{G_{defects}}{A} + \frac{G_{tears}}{A} \quad (5)$$

where A is the total membrane area, $G_{defects}$ is the total conductance through the defects, and G_{tears} is the total conductance through the tears. Although tears permit passage of both H^+ and K^+ ions, the Nafion surrounding the graphene raises the H^+/K^+ selectivity of tears to that of the Nafion. For simplicity, we approximate tears as holes covering a fraction, a, of the membrane area, all with the same diameter, D_{tear}. The tear conductance is then calculated as,

$$\frac{G_{tears}}{A} = \frac{a\sigma}{t + \frac{\pi}{4}D_{tear}} \quad (6)$$

The specific tear size distribution is not important in this modeling as different choices of D_{tear} and a can provide the same tear

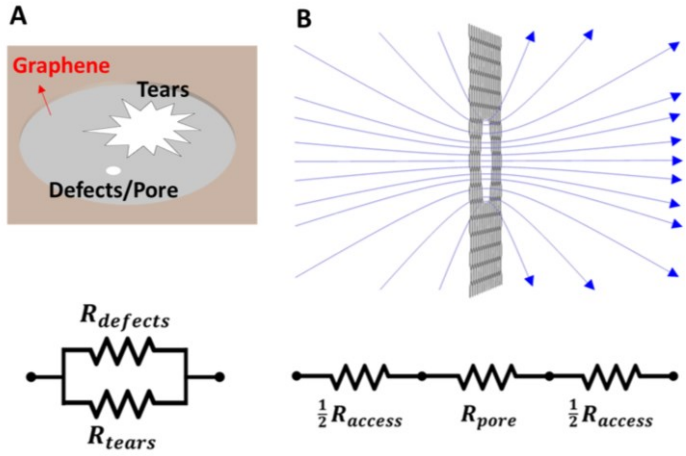

Fig. 5 Modelling ionic transport through centimeter-scale monolayer graphene membranes. A) Schematic and simplified resistance model with parallel conducting pathways through tears (R_{tears}) and defects ($R_{defects}$) in graphene with both large tears and defects/pore. B) Illustration of ion conduction through a graphene pore and corresponding resistance network accounting for access resistance (R_{access}) to reach and leave the hole on either side and the resistance to flow through the hole (R_{pore}).

conductance. Our interest is only in the order of magnitude of parameters required to explain the measurements.

Selectivity above that of the Nafion result from smaller intrinsic defects in graphene. Defects have a range of sizes that often resemble an exponential distribution,[75]

$$p(D) = \frac{1}{\overline{D}} e^{-D/\overline{D}} \quad (7)$$

where $p(D)$ is the probability density that a defect has diameter D and the parameter $\overline{D}$ determines the width of the distribution. We measured the areal density of defects larger than the etch test critical diameter to be $n_{>D_c} = 8.1 \times 10^6$ cm^{-2}, and enforce this requirement on the pore size distribution by defining the overall defect areal density, n, such that,

$$n \int_{D_c}^{\infty} p(D) dD = n_{>D_c} \quad (8)$$

This critical diameter, D_c, is between 0.5 and 1.0 nm but is not exactly known. We approximate it as the hydrated diameter of K^+, noting that the precise value is not critical to the order of magnitude of model parameters required to match the measured conductances. Summing the conductance over all defects gives,

$$\frac{G_{defects}}{A} = \int_{D_{ion}}^{\infty} \frac{n\sigma}{\frac{4t}{\pi(D - D_{ion})^2} + \frac{1}{D - D_{ion}}} p(D) dD \quad (9)$$

where D_{ion} is the ion diameter (taken as 0.66 nm for K^+ and 0 for H^+). Although deviations from this continuum resistance model are expected for nanometer-scale graphene pores,[37,75] these differences are much smaller than the orders of magnitude difference in conductance measured between micron- and centimeter-scale CVD graphene, and hence are neglected here. For sub-nm pores, precisely defining pore diameter is difficult, but in this model, it becomes the effective diameter providing the corresponding conductance from the continuum model.

Using a graphene thickness of $t = 0.68$ nm,[36] approximating tears as having diameter $D_{tear} = 0.2$ µm with $a = 0.11\%$ areal coverage, and choosing $\overline{D} = 0.8$ Å results in an H^+ conductance of 1.7 S/cm^2 (which agrees well with our experimentally measured value ~ 1.74 S/cm^2) and H^+/K^+ selectivity of 36.4, matching the measurements (Fig. 2G). This result corresponds to a defect areal density of $n = 3.3 \times 10^{10}$ cm^{-2}, similar to prior reports of graphene intrinsic defect densities.[58,75] Only 1.2×10^9 cm^{-2} of these defects are larger than helium (0.26 nm), consistent with the high quality of CVD graphene on these membranes as confirmed by the etch test. Although these very small defects would be impermeable to water and helium, and therefore perhaps not even counted as defects in other membrane applications, these defects would be proton permeable. The conductance of the pristine graphene lattice cannot explain the measured conductance of large area graphene: proton conduction through small defects does contribute significantly to transport.

However, conductance through small defects cannot entirely explain the transport. If tears were excluded from the model ($a = 0$), the density of defects larger than D_c would need to be ~100 times higher than measured by the etch test to match the measured conductances. This supports our supposition that tears contribute significantly to the conductances measured through larger area graphene. It further indicates that the H^+/K^+ selectivity in large area graphene could be increased significantly by reducing conductance through tears. In the micron-scale experiments, it was possible to isolate tear-free areas of graphene. Furthermore, defects in the graphene are not evenly spaced, as suggested by the etch test (Fig. 3B), instead having some clusters of higher defect density, *e.g.*, along wrinkles. This makes it possible to suspend low defectivity micron-scale areas of graphene and measure conductance through the graphene lattice.

The same graphene pore and tear densities, pore and tear size distributions, and conductance model can also explain the PCTE+Gr+IP+Nafion measurements. In this case, the Nafion is prepared in a different way, through a dip coating and curing process, resulting in a different thickness, conductivities and H^+/K^+ selectivity of the Nafion. Rather than defining several parameters to account for each of these structural complications in the measurements in Fig. 4B-D, we focus on the PCTE+Gr+IP+Nafion measurement, for which defects in the membrane and Nafion have been adequately sealed to provide selective ion transport. Since the graphene growth recipe was the same as for the N212|Gr|N212 membranes, we assume the same pore size distribution ($\overline{D}$), pore density (n), tear area fraction (a), and tear size (D_{tear}) as found for that membrane. The H^+ conductivity (σ_{H^+}) in the vicinity of the graphene is selected to match the measured PCTE+Gr+IP+Nafion conductivity and σ_{K^+} is chosen such that $\sigma_{H^+}/\sigma_{K^+}$ matches the measured PCTE+IP+Nafion selectivity of 15.9. For conductivities in the vicinity of the graphene of $\sigma_{H^+} = 1.7$ S/m (similar to the value of 1.6 S/m found for the N212|Gr|N212 membrane) and $\sigma_{K^+} = 0.11$ S/m, the conductance model predicts an overall PCTE+Gr+IP+Nafion H^+ areal conductance of 1.9 S/cm^2 (agrees well with our experimentally measured value ~ 1.85 S/cm^2) and H^+/K^+ selectivity of 24.5, matching the measurements. The ability to explain both the N212|Gr|N212 and PCTE+Gr+IP+Nafion measurements using the same graphene pore and tear densities and distributions serves as further validation for the conductance model and supports the conclusion that tears contribute significantly to conductances measured through centimeter-scale graphene.

Both tears and defect contribute appreciably to the measured conductance. With the low defect density of our CVD graphene, the measured conductances would not be as high without tears present. Similarly, ion selectivity above that of the bare Nafion would not be observed without sub-nanometer, ion sieving (proton selective) defects in the graphene. Although a number of approximations have been made in this analysis, the modeling shows that tears over a small fraction of the graphene area are responsible for the orders of magnitude differences in ion conductance measured between micron- and centimeter-scale areas of CVD graphene.

Conclusions

In conclusion, we systematically studied proton transport through atomically thin monolayer CVD graphene at the micron (within a graphene domain) and centimeter (across multiple

domains) scale. Larger defects (~1.6-50 nm) and tears (> 50nm) were found to contribute significantly towards the observed increase in areal proton conductance to ~1735 mS/cm^2 for the centimeter scale graphene membranes in comparison to the proton conductance of ~4.5-6 mS/cm^2 for micron scale graphene membranes. The corresponding increase in the areal conductance for K^+ ions (smallest ion with hydrated diameter of ~ 0.66 nm) from ~1mS/cm^2 (micron scale) to ~47.6 mS/cm^2 (centimeter scale) confirms the presence of defects for the centimeter scale CVD graphene transferred onto Nafion to form the graphene sandwich membrane. We deconvolute the contribution of larger defects and tears towards the proton conductivity by transferring graphene on to a well-defined porous PCTE support wherein tears and larger defects can be successfully isolated and sealed via interfacial polymerization (IP), thus minimizing their contribution. Atomically thin CVD graphene membranes supported on PCTE show areal proton conductance of ~3703 mS/cm^2 in comparison to areal proton conductance of ~1848 mS/cm^2 for graphene on PCTE after sealing defects and tears via IP. We develop a resistance-based transport model that is able to explain the observed conductivity for Nafion sandwich membranes as well as graphene on PCTE and we estimate ~0.11% areal fraction of non-selective larger defects and tears as well as sub-nanometer scale proton selective intrinsic defects to be responsible for the measured H^+ and K^+ conductivity values resulting in selectivity (ratio of H^+/K^+ conductivity) of ~14.2 for centimeter scale N212|Gr|N212 membranes and ~24.5 for PCTE+Gr+IP+Nafion membranes. We emphasize the thickness of PCTE+Gr+IP+Nafion membrane is ~14µm and yet it shows superior ionic selectivity ~24.5 compared to ~100µm thick N212||N212 with ionic selectivity ~8.8, while still maintaining comparable proton conductance. Finally, our work provides a new framework to test and evaluate H^+ conductance and selectivity of atomically thin 2D materials and highlights the importance of intrinsic sub-nanometer defects in selective proton permeation through large-area graphene atomically thin membranes for trasnformative applications in energy conversion/storage and novel separations.

Author Contributions

P.R.K. conceived and supervised the project. P.C. fabricated graphene membranes, material characterizations, and performed proton transport experiments in collaboration with N.M. P.C. fabricated PCTE supported graphene membrane. I.V synthesized graphene. M.S.H.B performed the transport model calculation and wrote the corresponding parts. All the authors were involved in analysis and discussions of the results. P.C. and P.R.K. wrote the manuscript with the input from all co-authors.

Conflicts of interest

P.R.K. acknowledges stake in a company aimed at commercializing 2D materials.

Acknowledgements

The use of Vanderbilt Institute of Nanoscale Science and Engineering CORE facilities are acknowledged. This work was supported in part by NSF CAREER award #1944134 in part and in part via faculty start-up funds from Vanderbilt University to P.R.K. This research is supported in part by the U.S. Department of Energy Isotope Program, managed by the Office of Science for Isotope R&D and Production under award number DE-SC0022237. We also acknowledge the ECS Toyota grant.

Notes and references

1 P. R. Kidambi, P. Chaturvedi and N. K. Moehring, *Science (80-.).*, 2021, 374, 7687.
2 O. Leenaerts, B. Partoens and F. M. Peeters, *Appl. Phys. Lett.*, 2008, **93**, 193107.
3 J. S. Bunch, S. S. Verbridge, J. S. Alden, A. M. van der Zande, J. M. Parpia, H. G. Craighead and P. L. McEuen, *Nano Lett.*, 2008, **8**, 2458–2462.
4 M. Miao, M. B. Nardelli, Q. Wang and Y. Liu, *Phys. Chem. Chem. Phys.*, 2013, **15**, 16132.
5 V. Berry, *Carbon N. Y.*, 2013, **62**, 1–10.
6 L. Tsetseris and S. T. Pantelides, *Carbon N. Y.*, 2014, **67**, 58–63.
7 M. Seel and R. Pandey, *2D Mater.*, 2016, **3**, 025004.
8 S. Hu, M. Lozada-Hidalgo, F. C. Wang, A. Mishchenko, F. Schedin, R. R. Nair, E. W. Hill, D. W. Boukhvalov, M. I. Katsnelson, R. A. W. Dryfe, I. V. Grigorieva, H. A. Wu and A. K. Geim, *Nature*, 2014, **516**, 227–230.
9 F. Banhart, J. Kotakoski and A. V. Krasheninnikov, *ACS Nano*, 2011, **5**, 26–41.
10 A. W. Robertson and J. H. Warner, *Nanoscale*, 2013, **5**, 4079.
11 P. Y. Huang, C. S. Ruiz-Vargas, A. M. van der Zande, W. S. Whitney, M. P. Levendorf, J. W. Kevek, S. Garg, J. S. Alden, C. J. Hustedt, Y. Zhu, J. Park, P. L. McEuen and D. a Muller, *Nature*, 2011, **469**, 389–92.
12 J. L. Achtyl, R. R. Unocic, L. Xu, Y. Cai, M. Raju, W. Zhang, R. L. Sacci, I. V. Vlassiouk, P. F. Fulvio, P. Ganesh, D. J. Wesolowski, S. Dai, A. C. T. van Duin, M. Neurock and F. M. Geiger, *Nat. Commun.*, 2015, **6**, 6539.
13 S. I. Yoon, D. J. Seo, G. Kim, M. Kim, C. Y. Jung, Y. G. Yoon, S. H. Joo, T. Y. Kim and H. S. Shin, *ACS Nano*, 2018, **12**, 10764–10771.
14 X. H. H. Yan, R. Wu, J. B. B. Xu, Z. Luo and T. S. S. Zhao, *J. Power Sources*, 2016, **311**, 188–194.
15 J. Liu, L. Yu, X. Cai, U. Khan, Z. Cai, J. Xi, B. Liu and F. Kang, *ACS Nano*, 2019, **13**, 2094–2102.
16 M. Lozada-Hidalgo, S. Zhang, S. Hu, A. Esfandiar, I. V Grigorieva and A. K. Geim, *Nat. Commun.*, 2017, **8**, 15215.
17 S. Bukola, Y. Liang, C. Korzeniewski, J. Harris and S. Creager, *J. Am. Chem. Soc.*, 2018, **140**, 1743–1752.
18 R. N. Karnik, *Nat. 2014 5167530*, 2014, **516**, 173–174.
19 P. R. Kidambi, R. A. Terry, L. Wang, M. S. H. Boutilier, D. Jang, J. Kong and R. Karnik, *Nanoscale*, 2017, **9**, 8496–8507.
20 X. Xu, Z. Zhang, J. Dong, D. Yi, J. Niu, M. Wu, L. Lin, R. Yin, M. Li, J. Zhou, S. Wang, J. Sun, X. Duan, P. Gao, Y. Jiang, X. Wu, H. Peng, R. S. Ruoff, Z. Liu, D. Yu, E. Wang, F. Ding and K. Liu, *Sci. Bull.*, 2017, **62**, 1074–1080.
21 T. Kobayashi, M. Bando, N. Kimura, K. Shimizu, K. Kadono, N. Umezu, K. Miyahara, S. Hayazaki, S. Nagai, Y. Mizuguchi, Y. Murakami and D. Hobara, *Appl. Phys. Lett.*, 2013, **102**, 023112.

22 P. R. Kidambi, D. D. Mariappan, N. T. Dee, A. Vyatskikh, S. Zhang, R. Karnik and A. J. Hart, *ACS Appl. Mater. Interfaces*, 2018, **10**, 10369–10378.

23 I. V. Vlassiouk, Y. Stehle, P. R. Pudasaini, R. R. Unocic, P. D. Rack, A. P. Baddorf, I. N. Ivanov, N. V. Lavrik, F. List, N. Gupta, K. V. Bets, B. I. Yakobson and S. N. Smirnov, *Nat. Mater.*, 2018, **17**, 318–322.

24 P. Cheng, N. K. Moehring, J. C. Idrobo, I. N. Ivanov and P. R. Kidambi, *Nanoscale*, 2021, **13**, 2825–2837.

25 P. Cheng, M. M. Kelly, N. K. Moehring, W. Ko, A. P. Li, J. C. Idrobo, M. S. H. Boutilier and P. R. Kidambi, *Nano Lett.*, 2020, **20**, 5951–5959.

26 P. R. Kidambi, D. Jang, J.-C. J.-C. Idrobo, M. S. H. M. S. H. Boutilier, L. Wang, J. Kong and R. Karnik, *Adv. Mater.*, 2017, **29**, 1700277.

27 P. R. Kidambi, M. S. H. M. S. H. Boutilier, L. Wang, D. Jang, J. Kim and R. Karnik, *Adv. Mater.*, 2017, **29**, 1605896.

28 M. I. Walker, P. Braeuninger-Weimer, R. S. Weatherup, S. Hofmann and U. F. Keyser, *Appl. Phys. Lett.*, 2015, **107**, 213104.

29 P. Chaturvedi, I. V. Vlassiouk, D. A. Cullen, A. J. Rondinone, N. V. Lavrik and S. N. Smirnov, *ACS Nano*, 2019, **13**, 12109–12119.

30 E. Griffin, L. Mogg, G. P. Hao, G. P. Hao, G. Kalon, G. Kalon, C. Bacaksiz, G. Lopez-Polin, G. Lopez-Polin, T. Y. Zhou, V. Guarochico, J. Cai, C. Neumann, A. Winter, M. Mohn, J. H. Lee, J. Lin, J. Lin, U. Kaiser, I. V. Grigorieva, K. Suenaga, B. Özyilmaz, H. M. Cheng, H. M. Cheng, W. Ren, A. Turchanin, F. M. Peeters, A. K. Geim and M. Lozada-Hidalgo, *ACS Nano*, 2020, **14**, 7280–7286.

31 L. Wang, M. S. H. Boutilier, P. R. Kidambi, D. Jang, N. G. Hadjiconstantinou and R. Karnik, *Nat. Nanotechnol.*, 2017, **12**, 509–522.

32 Z. Zeng, R. Song, S. Zhang, X. Han, Z. Zhu, X. Chen and L. Wang, *Nano Lett.*, 2021, acs.nanolett.1c00813.

33 Y. An, A. F. Oliveira, T. Brumme, A. Kuc and T. Heine, *Adv. Mater.*, 2020, **32**, 2002442.

34 S. Bukola, K. Beard, C. Korzeniewski, J. M. Harris and S. E. Creager, *ACS Appl. Nano Mater.*, 2019, **2**, 964–974.

35 S. Bukola, Z. Li, J. Zack, C. Antunes, C. Korzeniewski, G. Teeter, J. Blackburn and B. Pivovar, *J. Energy Chem.*, 2021, **59**, 419–430.

36 S. Garaj, W. Hubbard, A. Reina, J. Kong, D. Branton and J. A. Golovchenko, *Nature*, 2010, **467**, 190–193.

37 T. Jain, B. C. Rasera, R. J. S. Guerrero, M. S. H. Boutilier, S. C. O'Hern, J.-C. Idrobo and R. Karnik, *Nat. Nanotechnol.*, 2015, **10**, 1053–1057.

38 M. I. Walker, K. Ubych, V. Saraswat, E. A. Chalklen, P. Braeuninger-Weimer, S. Caneva, R. S. Weatherup, S. Hofmann and U. F. Keyser, *ACS Nano*, 2017, **11**, 1340–1346.

39 S. P. Surwade, S. N. Smirnov, I. V. Vlassiouk, R. R. Unocic, G. M. Veith, S. Dai and S. M. Mahurin, *Nat. Nanotechnol.*, 2015, **10**, 459–64.

40 H. Qi, Z. Li, Y. Tao, W. Zhao, K. Lin, Z. Ni, C. Jin, Y. Zhang, K. Bi and Y. Chen, *Nanoscale*, , DOI:10.1039/C8NR00050F.

41 L. Cantley, J. L. Swett, D. Lloyd, D. A. Cullen, K. Zhou, P. V Bedworth, S. Heise, A. J. Rondinone, Z. Xu, S. Sinton and J. S. Bunch, *Nanoscale*, 2019, **11**, 9856–9861.

42 L. Mogg, S. Zhang, G.-P. Hao, K. Gopinadhan, D. Barry, B. L. Liu, H. M. Cheng, A. K. Geim and M. Lozada-Hidalgo, *Nat. Commun.*, 2019, **10**, 4243.

43 A. Kusoglu and A. Z. Weber, *Chem. Rev.*, 2017, **117**, 987–1104.

44 C. L. Bentley, M. Kang, S. Bukola, S. E. Creager and R. Patrick, .

45 and S. S. Ivan Vlassiouk, Murari Regmi, Pasquale Fulvio, Sheng Dai, Panos Datskos, Gyula Eres, *ACS Nano*, 2011, **5**, 6069–6076.

46 I. Vlassiouk, P. Fulvio, H. Meyer, N. Lavrik, S. Dai, P. Datskos and S. Smirnov, *Carbon N. Y.*, 2013, **54**, 58–67.

47 I. Vlassiouk, S. Smirnov, M. Regmi, S. P. Surwade, N. Srivastava, R. Feenstra, G. Eres, C. Parish, N. Lavrik, P. Datskos, S. Dai and P. Fulvio, *J. Phys. Chem. C*, 2013, **117**, 18919–18926.

48 C. Gong, H. C. Floresca, D. Hinojos, S. McDonnell, X. Qin, Y. Hao, S. Jandhyala, G. Mordi, J. Kim, L. Colombo, R. S. Ruoff, M. J. Kim, K. Cho, R. M. Wallace and Y. J. Chabal, *J. Phys. Chem. C*, 2013, **117**, 23000–23008.

49 L. Lin, J. Zhang, H. Su, J. Li, L. Sun, Z. Wang, F. Xu, C. Liu, S. Lopatin, Y. Zhu, K. Jia, S. Chen, D. Rui, J. Sun, R. Xue, P. Gao, N. Kang, Y. Han, H. Q. Xu, Y. Cao, K. S. Novoselov, Z. Tian, B. Ren, H. Peng and Z. Liu, *Nat. Commun.*, 2019, **10**, 1–7.

50 Y.-C. Lin, C.-C. Lu, C.-H. Yeh, C. Jin, K. Suenaga and P.-W. Chiu, *Nano Lett.*, 2012, **12**, 414–419.

51 J. D. Wood, G. P. Doidge, E. A. Carrion, J. C. Koepke, J. A. Kaitz, I. Datye, A. Behnam, J. Hewaparakrama, B. Aruin, Y. Chen, H. Dong, R. T. Haasch, J. W. Lyding and E. Pop, *Nanotechnology*, 2015, **26**, 055302.

52 W. Xie, L. T. Weng, K. M. Ng, C. K. Chan and C. M. Chan, *Carbon N. Y.*, 2015, **94**, 740–748.

53 X. Liang, B. A. Sperling, I. Calizo, G. Cheng, C. A. Hacker, Q. Zhang, Y. Obeng, K. Yan, H. Peng, Q. Li, X. Zhu, H. Yuan, A. R. Hight Walker, Z. Liu, L. M. Peng and C. A. Richter, *ACS Nano*, 2011, **5**, 9144–9153.

54 M. Kratzer, B. C. Bayer, P. R. Kidambi, A. Matković, R. Gajić, A. Cabrero-Vilatela, R. S. Weatherup, S. Hofmann and C. Teichert, *Appl. Phys. Lett.*, 2015, **106**, 103101.

55 N. Petrone, C. R. Dean, I. Meric, A. M. Van Der Zande, P. Y. Huang, L. Wang, D. Muller, K. L. Shepard and J. Hone, *Nano Lett.*, 2012, **12**, 2751–2756.

56 M. E. Suk and N. R. Aluru, *J. Chem. Phys.*, 2014, **140**, 1–7.

57 R. C. Rollings, A. T. Kuan and J. A. Golovchenko, *Nat. Commun.*, 2016, **7**, 11408.

58 M. S. H. Boutilier, C. Sun, S. C. O'Hern, H. Au, N. G. Hadjiconstantinou and R. Karnik, *ACS Nano*, 2014, **8**, 841–849.

59 C. A. Schneider, W. S. Rasband and K. W. Eliceiri, *Nat. Methods*, 2012, **9**, 671–675.

60 M. Tesfaye, D. I. Kushner, B. D. McCloskey, A. Z. Weber and A. Kusoglu, *ACS Macro Lett.*, 2018, **7**, 1237–1242.

61 and H. C. Duhee Yoon, Young-Woo Son, *Nano Lett.*, 2011, **11**, 3227–3231.

62 A. C. Ferrari and D. M. Basko, *Nat. Nanotechnol.*, 2013, **8**, 235–246.

63 P. R. Kidambi, B. C. Bayer, R. Blume, Z.-J. Wang, C. Baehtz, R. S. Weatherup, M.-G. Willinger, R. Schloegl and S. Hofmann, *Nano Lett.*, 2013, **13**, 4769–4778.

64 P. R. Kidambi, C. Ducati, B. Dlubak, D. Gardiner, R. S. Weatherup, M.-B. Martin, P. Seneor, H. Coles and S. Hofmann, *J. Phys. Chem. C*, 2012, **116**, 22492–22501.

65 L. Wang, C. M. C. M. Williams, M. S. H. M. S. H. Boutilier, P. R. Kidambi and R. Karnik, *Nano Lett.*, 2017, **17**, 3081–3088.

66 M. S. H. Boutilier, D. Jang, J.-C. Idrobo, P. R. Kidambi, N. G.

Hadjiconstantinou and R. Karnik, *ACS Nano*, 2017, **11**, 5726–5736.

67 P. R. Kidambi, G. D. Nguyen, S. Zhang, Q. Chen, J. Kong, J. Warner, A.-P. Li and R. Karnik, *Adv. Mater.*, 2018, **1804977**, 1804977.

68 S. Sanders, A. Cabrero-Vilatela, P. R. Kidambi, J. A. Alexander-Webber, C. Weijtens, P. Braeuninger-Weimer, A. I. Aria, M. M. Qasim, T. D. Wilkinson, J. Robertson, S. Hofmann and J. Meyer, *Nanoscale*, , DOI:10.1039/c5nr03246f.

69 D. Perconte, F. A. Cuellar, C. Moreau-Luchaire, M. Piquemal-Banci, R. Galceran, P. R. Kidambi, M.-B. Martin, S. Hofmann, R. Bernard, B. Dlubak, P. Seneor and J. E. Villegas, *Nat. Phys.*, 2017, **14**, 25–29.

70 R. Wang, P. R. P. R. Whelan, P. Braeuninger-Weimer, S. Tappertzhofen, J. A. J. A. Alexander-Webber, Z. A. Z. A. Van Veldhoven, P. R. Kidambi, B. S. B. S. Jessen, T. Booth, P. Bøggild and S. Hofmann, *ACS Appl. Mater. Interfaces*, 2016, **8**, 33072–33082.

71 P. R. Kidambi, C. Weijtens, J. Robertson, S. Hofmann and J. Meyer, *Appl. Phys. Lett.*, 2015, **106**, 063304.

72 C. Casiraghi, *Phys. Rev. B - Condens. Matter Mater. Phys.*, 2009, **80**, 2–4.

73 Y. Liu, L. Gao, J. Sun, Y. Wang and J. Zhang, *Nanotechnology*, 2009, **20**, 465605.

74 S. J. Kwon, T. H. Han, T. Y. Ko, N. Li, Y. Kim, D. J. Kim, S. H. Bae, Y. Yang, B. H. Hong, K. S. Kim, S. Ryu and T. W. Lee, *Nat. Commun.*, 2018, **9**, 1–9.

75 S. C. O'Hern, C. A. Stewart, M. S. H. H. Boutilier, J. C. Idrobo, S. Bhaviripudi, S. K. Das, J. Kong, T. Laoui, M. Atieh, R. Karnik, S. C. O'Hern, C. A. Stewart, M. S. H. H. Boutilier, J. C. Idrobo, S. Bhaviripudi, S. K. Das, J. Kong, T. Laoui, M. Atieh and R. Karnik, *ACS Nano*, 2012, **6**, 10130–10138.

